Electronic supplementary information (ESI) for

Dimerization of sub-Nanoscale molecular clusters affords Broadly Tunable Viscoelasticity above Glass Transition Temperature

Xin Zhou,[a] Junsheng Yang,*[a] Jia-Fu Yin,[a] Wei Liu-Fu,[a] Jiayi Huang,[a] Mu Li,[a] Yuan Liu,[a] Linkun Cai,[a] Tao Lin Sun[a] and Panchao Yin*[a]

* Corresponding author E-mail: yinpc@scut.edu.cn, jsyang20@scut.edu.cn

1. Materials and Methods

Materials. Dichloromethane (DCM), tetrahydrofuran (THF), N, N- dimethyllformamide (DMF) and toluene were dried by refluxing under nitrogen atmosphere with calcium hydroxide and distilled. Other stated solvents were purchased from commercial sources and used without further purification. Chemical reagents used in this work were provided by various chemical reagent industries. Cuprous bromide (CuBr) was purified by washing with acetic acid and acetone then dried under vacuum. All the reactions were performed in dried glasswares under N_2 environment. Silica gel (230-400 mesh) was used as stationary phase during flash column chromatography process.

Nuclear Magnetic Resonance (NMR) Spectroscopy. All the samples were dissolved in deuterium solvents with tetramethylsilane (TMS) as reference. NMR spectra were recorded on Bruker AVANCE II 500 spectrometer at 298 k.

Small Angle X-ray Scattering (SAXS). The scattering vector q is calculated to be $q = 4\pi (\sin\theta) / \lambda$, while the scattering angle is 2θ. The exposure time was set to be 100 s for solution samples and 10 s for solid samples to acquire the structural information. Data analysis was processed with Fit 2D software and the background scattering was subtracted.

Differential Scanning Calorimetry (DSC). Thermal property was determined with a NETZSCH DSC214 instrument. The temperature ranges were -50 ℃ to 100 ℃ with a heating rate of 10 C/min. All the tests were performed under N_2 atmosphere.

Gel Permeation Chromatography (GPC). Dimers and OPOSS-Vinyl were dispersed in HPLC THF solvent and then subjected to GPC instrument equipped with automatic injection system, LC-100 column oven, polystyrene gel columns and UV detector. Monodispersed polystyrene was used as standard to quantify the molecule weight of each sample.

Matrix-assisted laser desorption/ionization time-of-flight mass spectrometry (MALDI-TOF MS). MALDI-TOF measurements were carried out on a Bruker autoflex III smartbean. In the sample preparation, *trans*-2-(3-(4-*t*-butyl-phenyl)-2-methyl-2-propenylidene)malononitrile (DCTB) matrix (20 mg/mL in THF) and cationizing agent NaTFA (10 mg/mL in THF) were mixed in the ratio of 10/1 (v/v). Samples were dissolved in THF at a concentration of 5 mg/ml.

Rheology. A controlled-stress rotational rheometer (Anton Paar MCR-302) with parallel plate geometry was used to investigate the rheological properties of OPOSS-Vinyl and Dimers. Rheological frequency sweep test was performed from 1 to 200 Hz with a shear strain of 0.5% at different temperatures (0 ℃ to 60 ℃). The dynamic properties, including storage modulus, loss modulus and loss factor, were obtained from the measurements.

Dielectric test. The dielectric performances were studied by using the Novocontrol broadband dielectric converter with temperature control equipment. The broadband dielectric spectra were recorded under gradient frequency from 10^{-1} Hz to 10^{7} Hz while the testing temperature were fixed (40 ℃ to 180℃).

HN function fitting. The complex loss modulus (M") of the relaxation can be well fitted by using the general Havriliak−Negami (HN) function:

$$M^*(\omega) = M_\infty\left(1 - \frac{1}{\left(1 + (i\omega\tau_M)^\alpha\right)^\beta}\right)$$

where the parameter M_∞ is the loss modulus at the high-frequency limit and τ_M is the relaxation time. The exponents $0 < \alpha$, $\alpha\beta \leq 1$ are the shape parameters, describing the symmetric and asymmetric broadening of the complex dielectric function.

VFT fitting. As several steps (α, β or γ relaxation) were involved in a dielectric relaxation process, broadband dielectric spectrum gave a combination of multiple peaks and the exact location of certain peak was hard to be determined. The corresponding frequency of each relaxation peak was subsequently defined by means of the peak-differentiation-imitating analysis based on the **Havriliak-Negami (HN) equation.** Vogel-Fulcher-Tammann (VFT) ($f = f_0 \exp(-B/(T-T_0))$ equation was used for the fitting operation and the fitting pattern was found to match well with the experimental data points (Fig. S8). Then, the dynamic fragility value for OPOSS-MOP was calculated to be 83 based on the mentioned function ($m = \frac{B/T_g}{(ln10)(1 - T_0/T_g)^2}$)

WLF fitting of the shifting factors (α_T). Shifting factors were collected based on the horizontal shifting distance of SAOS data under different temperature (The reference temperature was set to be 50°C. WLF equation $\left(log\alpha_T = \frac{-C_1(T - T_s)}{C_2 + T - T_s}\right)$ was applied to monitor the variation trend of shifting factors toward the testing temperature. For the WLF formula, T_s denoted the reference temperature and C_1, C_2 represented two empirical constant. The fitting operation was carried out with the Gravity software. The fitting curves all matched well with the experimental data points.

Molecular dynamics (MD) simulations. All-atom molecular dynamics simulations were used in the current work. Structural model of dimers with different linkers was established on the basis of the Materials Studio and LAMMPS software package. Our simulation cell contained 64 molecules. The time step was 1 fs and the cutoff distance is 9.5 Å for our calculations. COMPASS force field was applied to dimer molecules to describe the inter- and intra-atomic interactions. In order to ensure the dimer system reaching equilibrium at the chosen temperatures, the sample was pretreated for 2 ns with an NPT ensemble (p = 1 bar, T = 500 K). Then, dimer system was gradually cooled to 300K. The corresponding mean square displacement (MSD) and diffusion coefficient data were collected to elucidate the structural dynamics of dimer molecules.

2. Supporting Figures

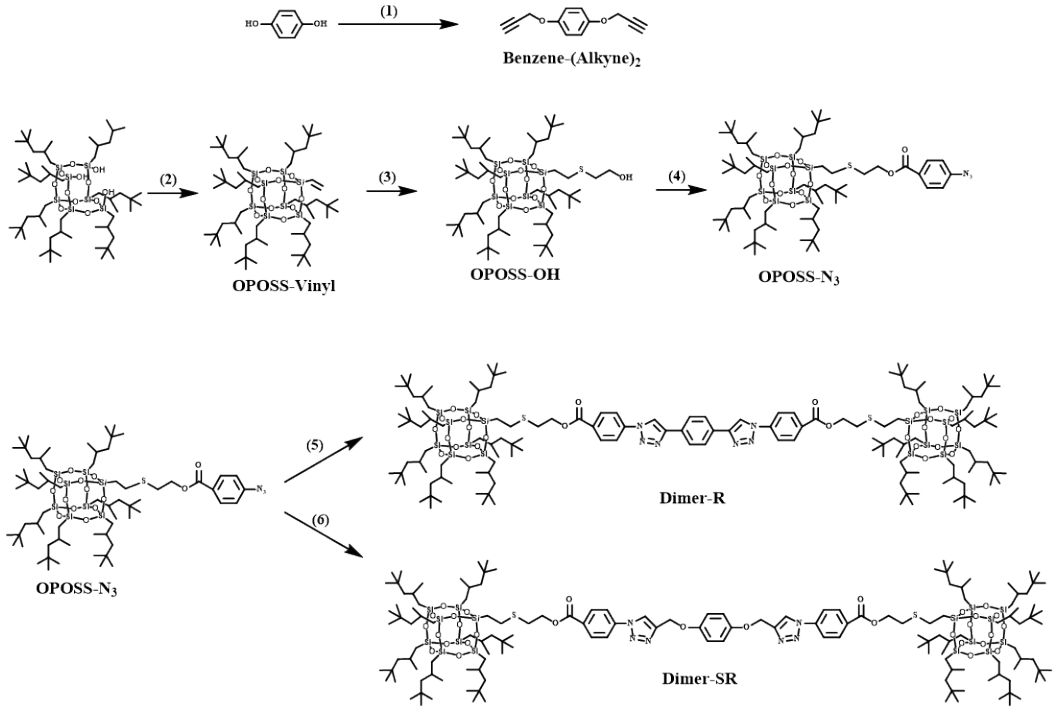

Scheme S1. Synthetic routes for Dimer-SR and Dimer-R. (1) Propargyl bromide, K_2CO_3, Acetone, 65 °C; (2) Trichlorovinylsilane, TEA, THF, RT; (3) 2-mercaptoethanol, Irgacure 2959, UV 365 (10 min), THF, RT; (4) 4-Azidobenzoic acid, DMAP, DIPC, THF, RT. (5) 1,4-Diethynylbenzene, CuBr, PMDETA, Toluene, RT; (6) Benzene-(alkyne)$_2$, CuBr, PMDETA, Toluene, RT.

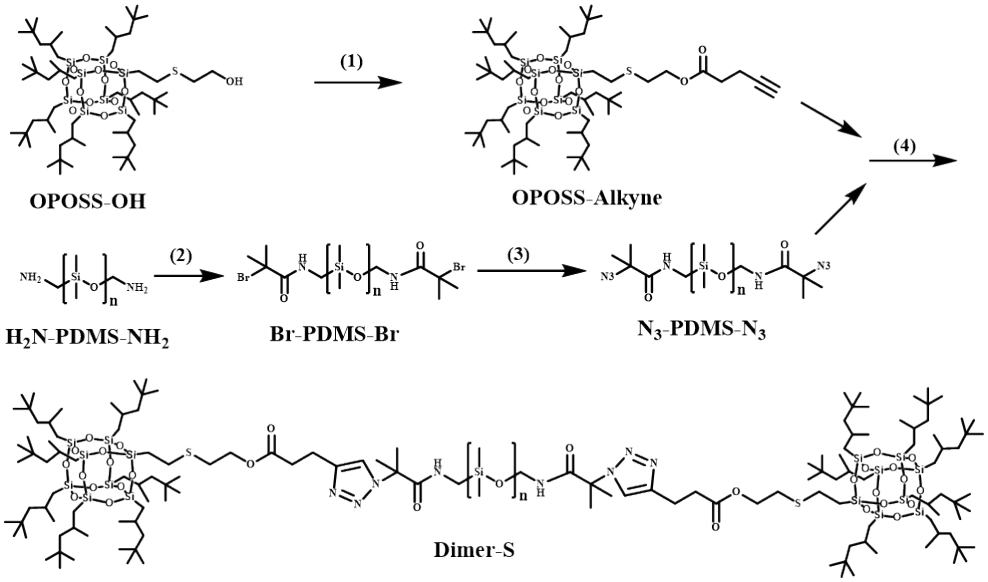

Scheme S2. Synthetic routes for Dimer-S. (1) 4-Pentynoic acid, DMAP, DIPC, THF, RT; (2) 2-bromo-2-methylpropanoyl bromide, TEA, DCM, RT; (3) Sodium azide, DMF/toluene, 80 °C; (4) CuBr, PMDETA, Toluene, RT;

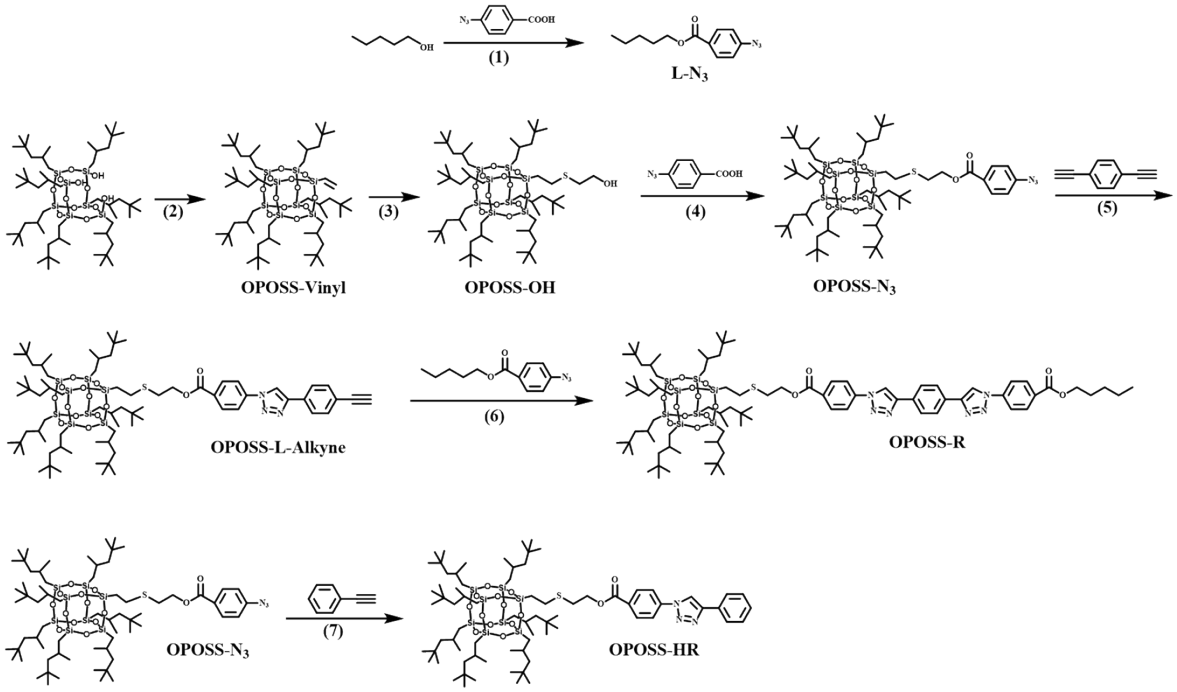

Scheme S3. Synthetic routes for OPOSS-HR and OPOSS-R. (1) 4-Azidobenzoic acid, DMAP, DIPC, THF, RT. (2) Trichlorovinylsilane, TEA, THF, RT; (3) 2-mercaptoethanol, Irgacure 2959, UV 365 (10 min), THF, RT; (4) 4-Azidobenzoic acid, DMAP, DIPC, THF, RT. (5) 1,4-Diethynylbenzene, CuBr, PMDETA, Toluene, RT; (6) L-N_3, CuBr, PMDETA, Toluene, RT. (7) Phenylacetylene, CuBr, PMDETA, Toluene, RT.

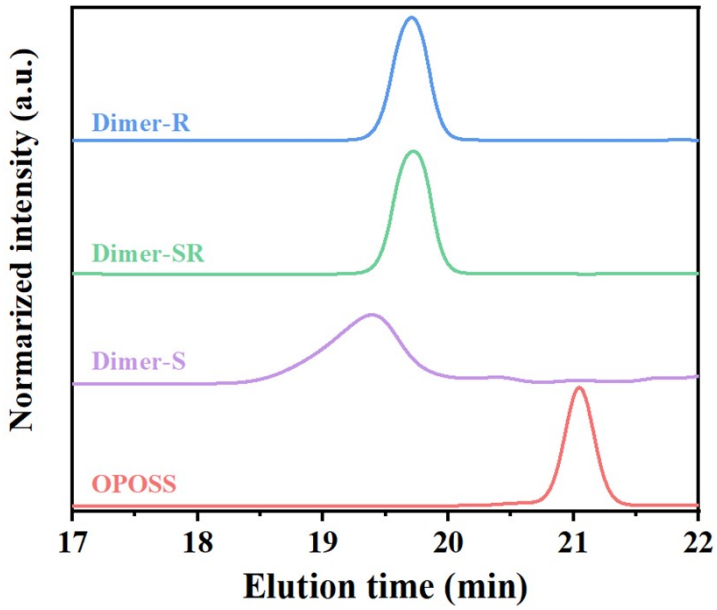

Fig. S1. GPC data for OPOSS and OPOSS dimers.

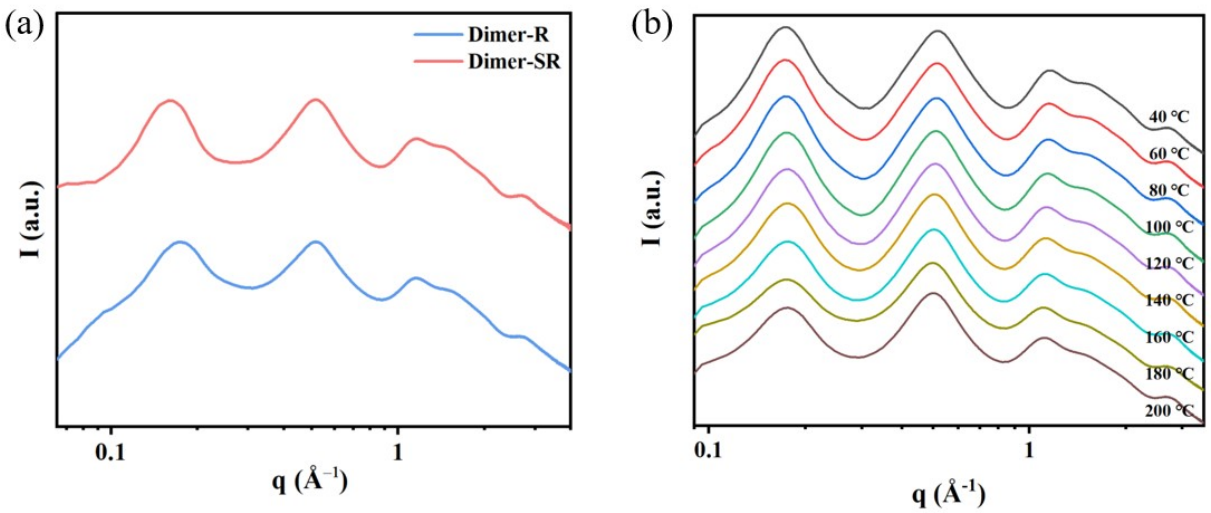

Fig. S2. (a) Small angle X-ray scattering (SAXS) of dimer molecules after 3 months of placement. (b) Temperature-dependent SAXS experiments for Dimer-R from 40-200 °C.

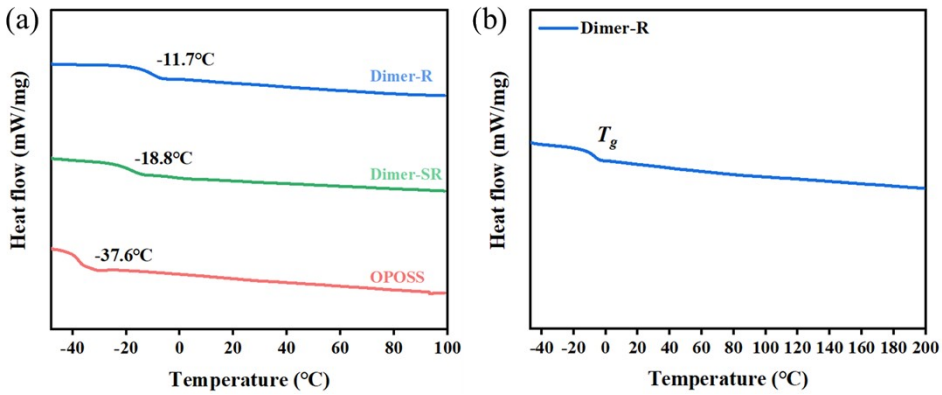

Fig. S3. (a) DSC data for OPOSS and OPOSS dimers from -50-100 °C. (b) DSC data for Dimer-R from -50-200 °C.

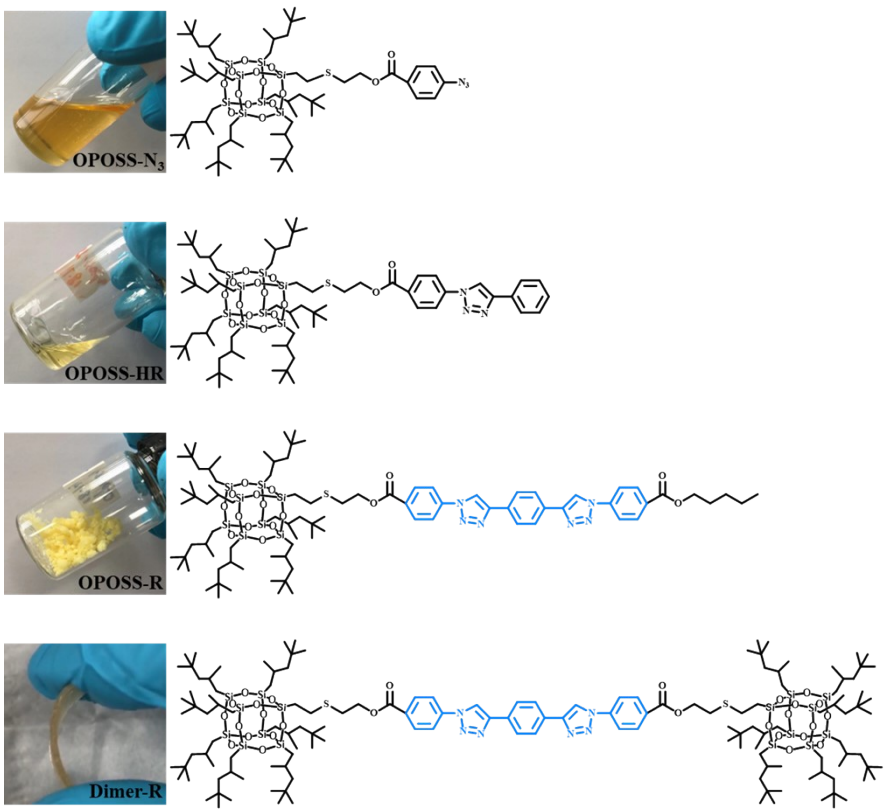

Figure S4. The physical appearance and molecular structures of OPOSS monomers and Dimers.

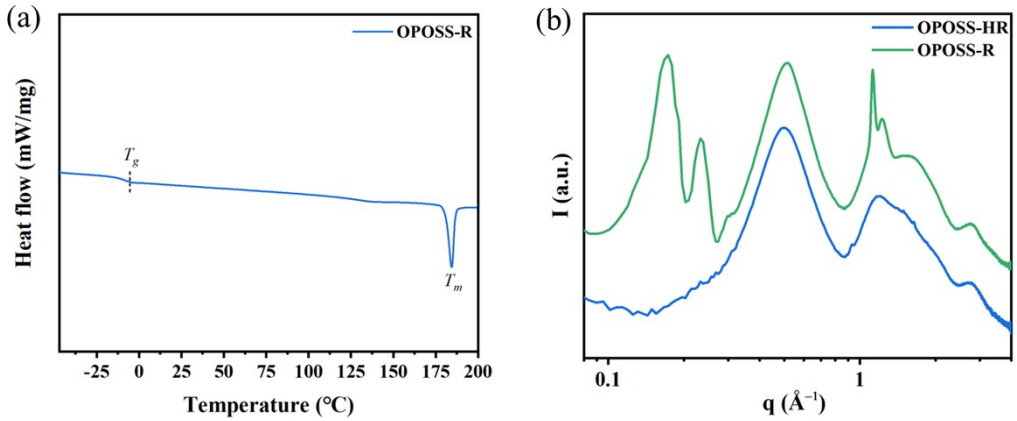

Figure S5. (a) DSC data of OPOSS-R. Melting peak (T_m) indicated the obvious crystallization of OPOSS-R. (b) Small angle X-ray scattering (SAXS) of OPOSS-HR and OPOSS-R. Melting peak (T_m) and crystallization peaks indicated the obvious crystallization of OPOSS-R.

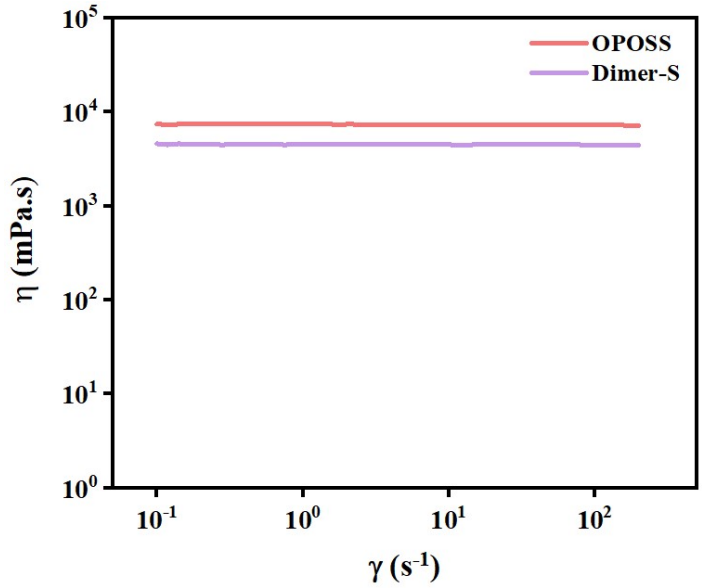

Fig. S6. Viscosity shear rate curves of OPOSS and Dimer-S.

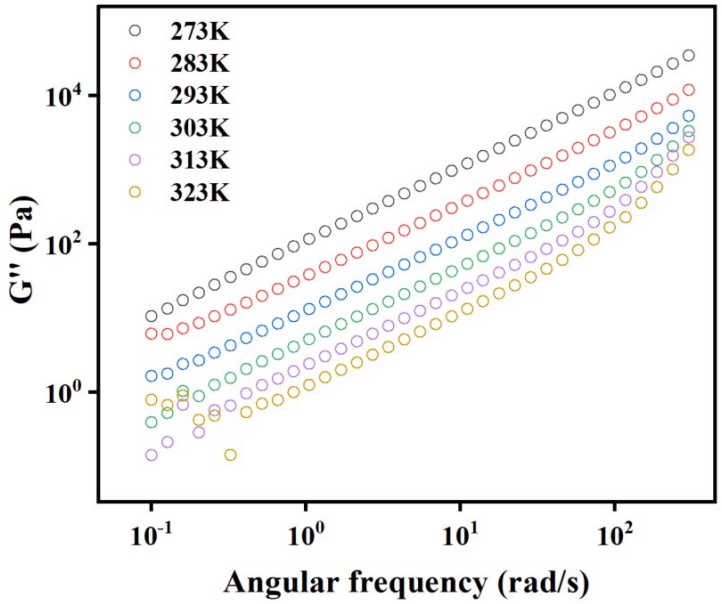

Fig. S7. SAOS raw data for OPOSS.

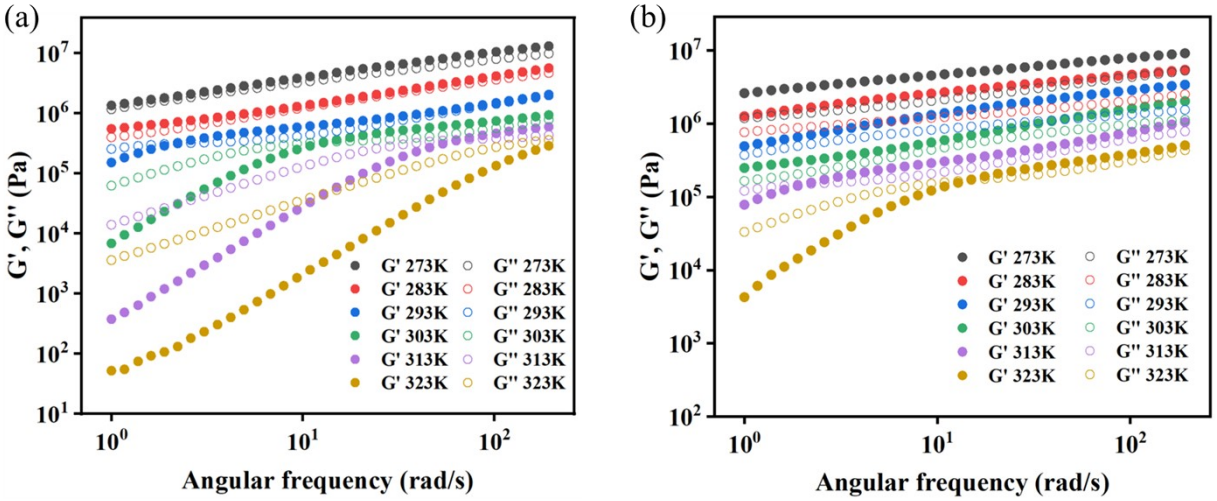

Fig. S8. SAOS raw data for (a) Dimer-SR and (b) Dimer-R.

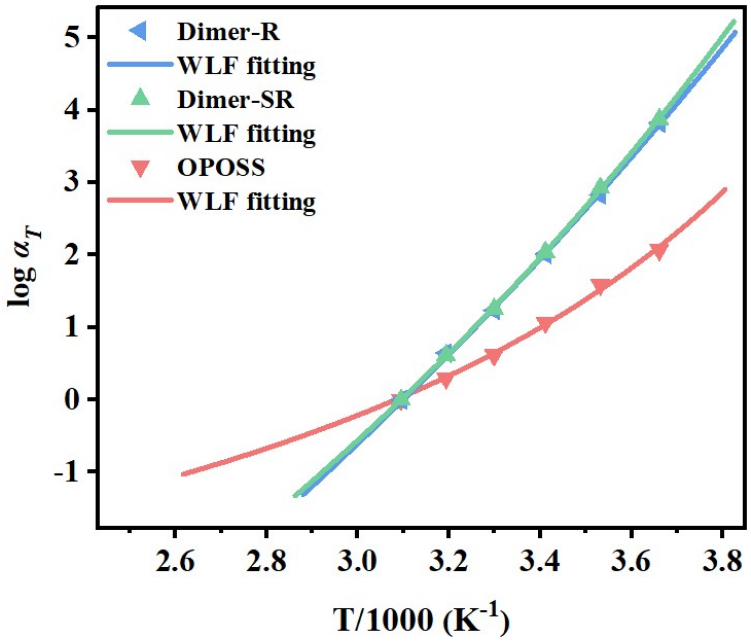

Fig. S9. Time-temperature superposition shifting factors (a_T) and WLF fitting profiles for OPOSS and OPOSS dimers.

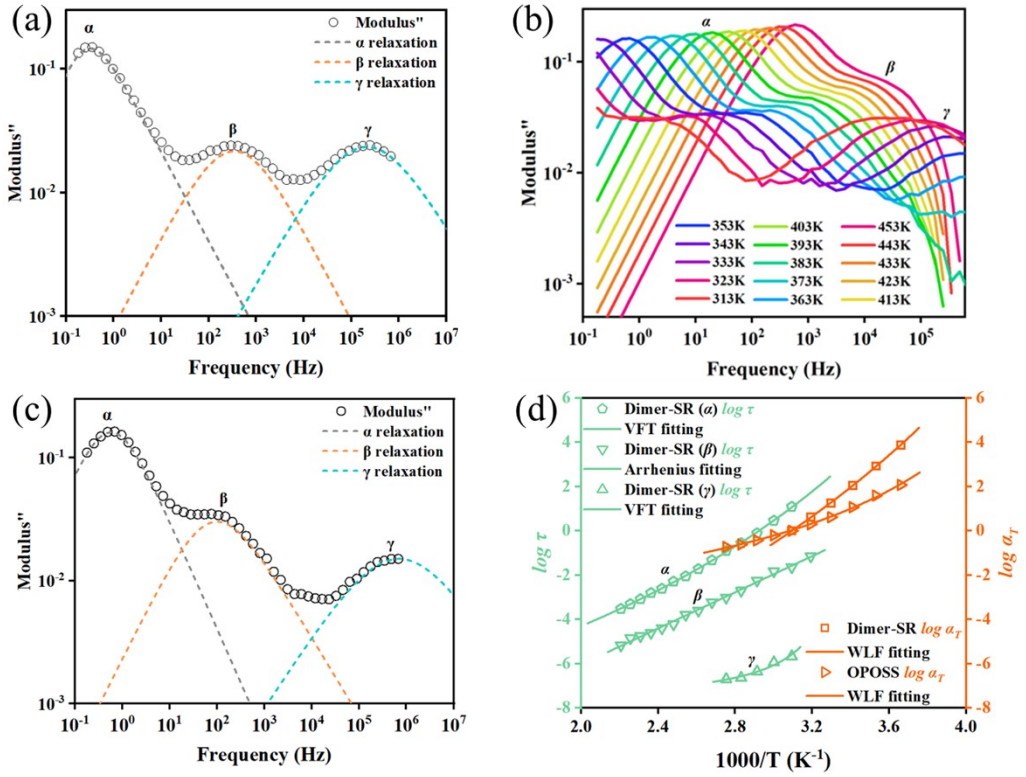

Fig. S10. The dielectric measurement for Dimer-R and Dimer-SR. (a) Peak-differentiation-imitating analysis for the broadband loss modulus spectra of Dimer-R at 373K based on the Havriliak-Negami (HN) function. (b) The dielectric spectrum of Dimer-SR from 313K to 453K. (c) Peak-differentiation-imitating analysis for the broadband loss modulus spectra of Dimer-SR at 353K based on the Havriliak-Negami (HN) function. (c) Integrated diagram of shifting factors (α_T) for different samples and relaxation time (τ) for multiple relaxation processes.

The relaxation time (τ) obtained from the Peak-differentiation-imitating analysis were fitted by classical VFT or Arrhenius equations. α and γ relaxations were well fitted by VFT equations while β relaxation was well fitted Arrhenius function.

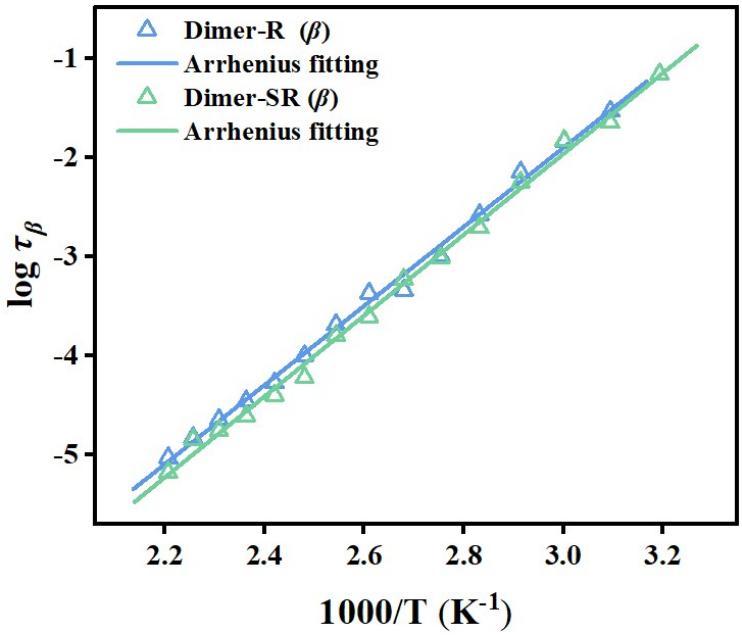

Fig. S11. The temperature dependences of the characteristic β relaxation time for Dimer-SR and Dimer-R.

Table S1. Activation energy (β relaxation) of dimers

	Dimer-R	Dimer-SR
E_a (KJ/mol)	76.38	78.08

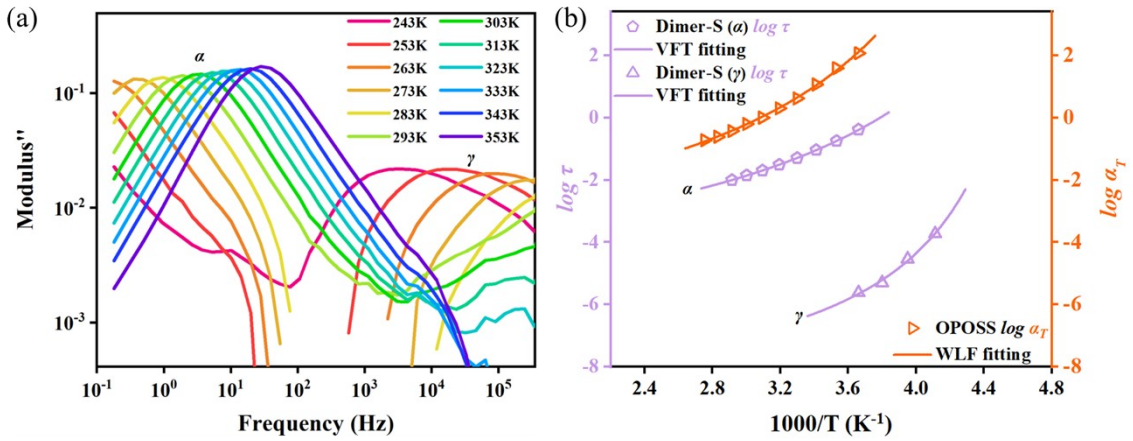

Fig. S12. The dielectric measurement for Dimer-S. (a) The dielectric spectrum of Dimer-S from 243K to 353K. (b) Integrated diagram of shifting factors (α_T) for different samples and relaxation time (τ) for multiple relaxation processes.

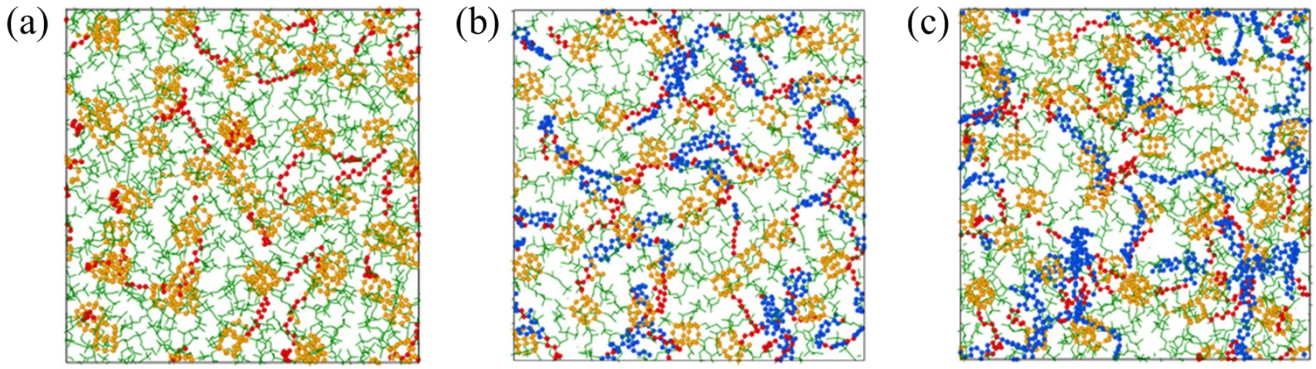

Fig. S13. Slice of molecular packed of different dimers from MD simulations. (a) Dimer-S. (b) Dimer-SR. (c) Dimer-R.

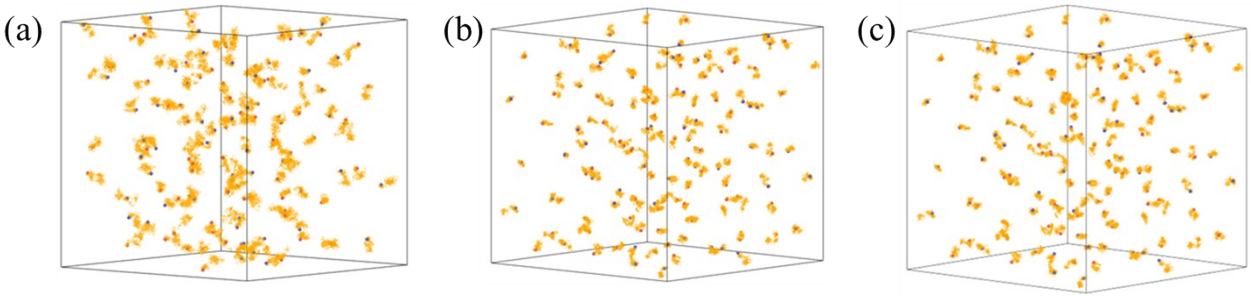

Fig. S14. Center-of-mass motion trajectories of OPOSS of different dimers from 0-7 ns by MD simulations. (a) Dimer-S. (b) Dimer-SR. (c) Dimer-R.

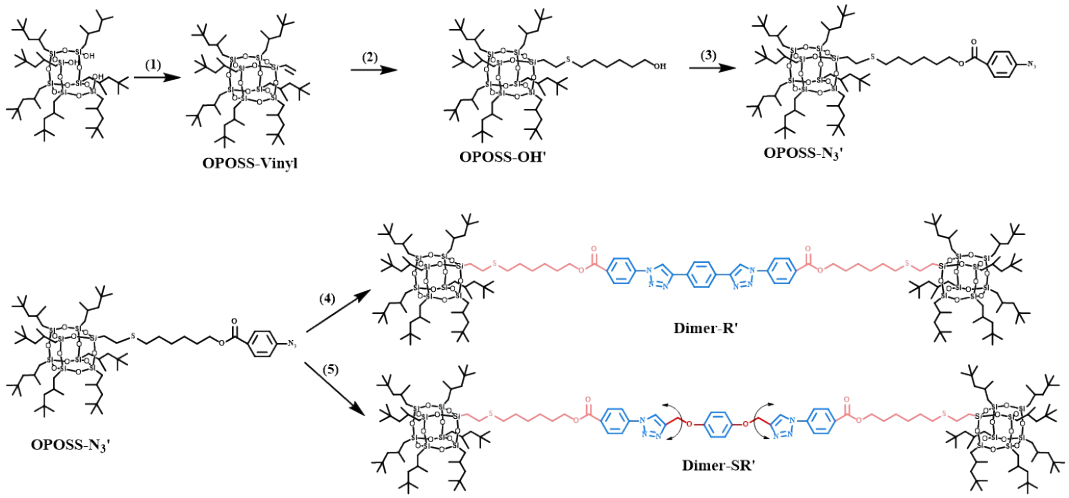

Scheme S4. Synthetic routes for Dimer-SR' and Dimer-R'. (1) Trichlorovinylsilane, TEA, THF, RT; (3) 6-Mercapto-1-hexanol, Irgacure 2959, UV 365 (10 min), THF, RT; (3) 4-Azidobenzoic acid, DMAP, DIPC, THF, RT. (5) 1,4-Diethynylbenzene, CuBr, PMDETA, Toluene, RT; (6) Benzene-(alkyne)$_2$, CuBr, PMDETA, Toluene, RT.

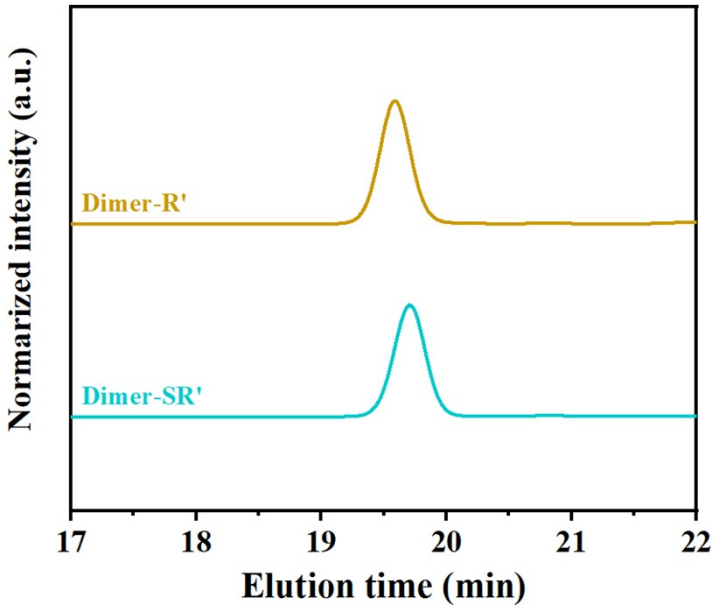

Fig. S15. GPC data for Dimer-SR' and Dimer-SR'.

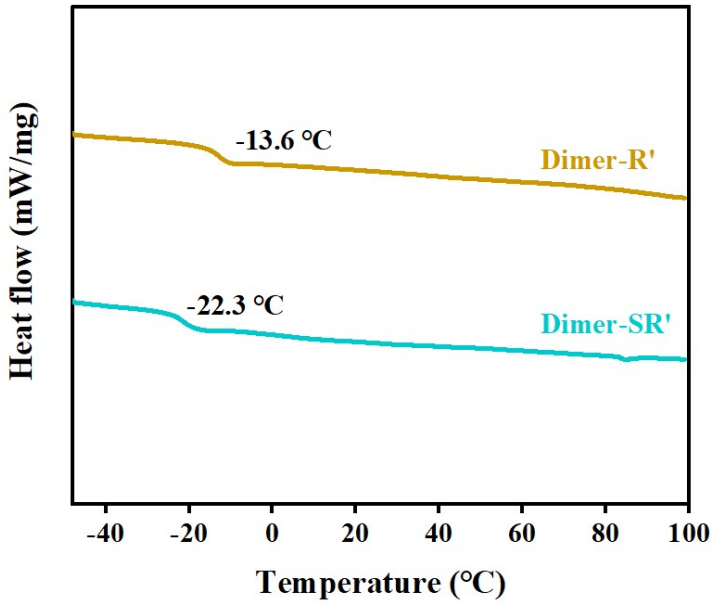

Fig. S16. DSC data of Dimer-SR' and Dimer-R'.

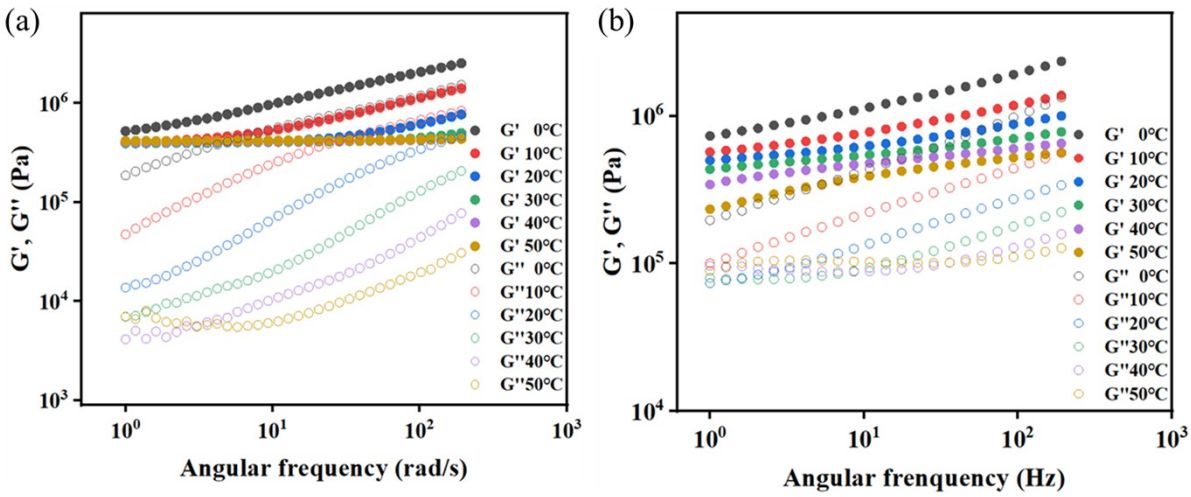

Fig. S17. SAOS raw data for (a) Dimer-SR' and (b) Dimer-R'.

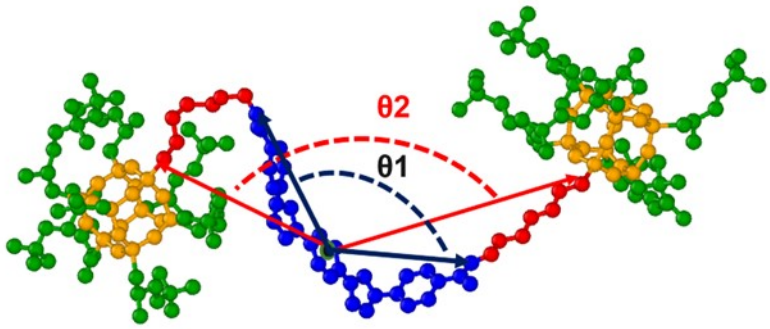

Fig. S18. Definition of the rotational stiffness and flexural resistance of dimer linker.

Table S2. Rotational stiffness (-cosθ1 and -cosθ2), molecular size (R_{ee} and R_g) parameters and viscosity (η) of different dimers.

Simples	-cos(θ_1)	-cos(θ_2)	R_{ee} (Å)	R_g (Å)	η (mPa.s)
Dimer-R	0.4540	0.0286	20.32	11.89	30.05
Dimer-SR	0.1848	-0.0724	20.15	11.86	26.20
Dimer-R’	0.4486	-0.0700	20.21	12.03	28.53
Dimer-SR’	0.2986	-0.0193	21.79	12.70	28.50

Table S3. Van der Waals(E_{VdW}), bond stretching (E_{bond}), bond bending (E_{angle}) and torsional (E_{dihed}) interactions of different dimer molecular system.

Simples	E_{VdW}(kcal/mol)	E_{bond}(kcal/mol)	E_{angle}(kcal/mol)	E_{dihed}(kcal/mol)

Dimer-R	-2680.610	13061.288	20560.802	-1824.317
Dimer-SR	-2917.810	13150.369	20718.645	-11243.216
Dimer-R’	-2680.511	13233.779	20912.031	-2531.816
Dimer-SR’	-2834.142	13335.314	21134.057	-11978.979

3. Synthesis procedures

3.1 OPOSS-vinyl (OPOSS)

Trisilanol-isooctyl POSS (11.8g, 10 mmol), and TEA (4.6 mL, 33mmol) were fully dissolved in 100 mL freshly dried THF, then the mixture was cooled to 0 °C. With stirring, Trichlorovinylsilane (1.4 mL, 11 mmol) was added dropwise into the mixture. The resulting mixture was stirred for 14 h at room temperature. After that, the white precipitate was filtered out, and the filtrate was evaporated by rotary evaporation. The crude product was further purified by flash column chromatography on silica gel with pure PE as the eluent to afford OPOSS-vinyl (7.80g, 63%) as a clear viscous liquid.

3.2 OPOSS-OH

OPOSS-vinyl (5.0 g, 4.05 mmol) and 2-mercaptoethanol (468 mg, 6.0 mmol) were dissolved in 30 mL THF. Then, photoinitiator (Irgacure 2959) (13.4 mg, 0.06 mmol) was added to the solution. The solution was irradiated by the 365 nm UV light for 15 min. The crude product was purified by silica gel chromatography with DCM: PE (1: 1, v/v) to afford OPOSS-OH (3.67g, 69%) as a clear viscous liquid.

3.3 OPOSS-Alkyne

OPOSS-OH (6.0 g, 4.57mol), 4-Pentynoic acid (672 mg, 6.86 mmol) and DMAP (104.9 mg, 0.86mmol) were added followed by the addition of 50 mL freshly dried THF to dissolved the reactant. Then the mixture was cooled to 0 °C. With stirring, DIPC (1.06 mL, 6.86 mmol) was added dropwise into the mixture. The resulting mixture was stirred for 24 h at room temperature. Then the THF was fully removed by rotary evaporation afford the crude product. The crude product was further purified by flash column chromatography on silica gel with PE and DCM mixture (v/v = 3:1) as the eluent to afford OPOSS-Alkyne (4.5 g, 70%) as a clear viscous liquid.

3.4 OPOSS-OH'

OPOSS-vinyl (10.0 g, 8.1 mmol) and 6-mercapto-1-hexanol (1.34 g, 10.0 mmol) were dissolved in 50 mL THF. Then, photoinitiator (Irgacure 2959) (22.4 mg, 0.10 mmol) was added to the solution. The solution was irradiated by the 365 nm UV light for 15 min. The crude product was purified by silica gel chromatography with DCM: PE (1: 1, v/v) to afford OPOSS-OH' (7.5 g, 67%) as a clear viscous liquid.

3.5 Br-PDMS-Br

H_2N-PDMS-NH_2 (5.0 g, 3.3 mmol, M_W=1500) and TEA (4.6 mL, 33mmol) were fully dissolved in 100 mL DCM. Then the mixture was cooled to 0 °C. With stirring, 2-bromo-2-methylpropanoyl bromide (4.05 mL, 33 mmol) was added dropwise into the mixture. The resulting mixture was stirred protected from light for 24 h at room temperature. After that, precipitate was filtered out, and the filtrate was dropped into a beaker containing 400 mL of a mixture of methanol and water (v:v=1:1) under stirring. Then the organic phase was collected and after repeating this operation three times, the organic phase was dried with anhydrous sodium sulfate to afford Br-PDMS-Br (3.9 g, 78%) as a clear viscous liquid.

3.6 N_3-PDMS-N_3

Br-PDMS-Br (0.84 g, 0.47 mmol and sodium azide (0.514g, 7.9 mmol) were added to a mixture of DMF (15ml) and toluene (28ml) . Then the solution was stirred at 80 °C under a nitrogen atmosphere for 16 h. After that, The reaction solution was poured into 100 mL deionised water with stirring. Then the organic phase was washed 3 times with 100 mL deionised water and dried with anhydrous sodium sulphate to afford N_3-PDMS-N_3 (605 mg, 72%) as a clear viscous liquid.

3.7 Dimer-S

N_3-PDMS-N_3 (500 mg, 0.28mmol), OPOSS-Alkyne (950 mg, 0.68 mmol) and CuBr (6 mg, 0.042 mmol) were added to a flask and then transferred to glove box. 10 mL Toluene was added to dissolve the reagents. Then PMDETA (7 mg, 0.040 mmol) was successively introduced. The reaction was performed at room temperature with stirring for 18 h in glove box. After that, the reaction mixture was subjected to column chromatography with PE: EA (4:1, v/v) to Dimer-S (550 mg, 43%) as a clear viscous liquid.

3.8 OPOSS-N_3

OPOSS-OH (8.0 g, 6.1 mmol), 4-Azidobenzoic acid (1.98 g, 12.2 mmol) and DMAP (146.4 mg, 1.2mmol) were added followed by the addition of 50 mL freshly dried THF to dissolved the reactant. Then the mixture was cooled to 0 °C. With stirring, DIPC (1.89 mL, 12.2 mmol) was added dropwise into the mixture. The resulting mixture was stirred for 24 h at room temperature. Then the THF was fully removed by rotary evaporation afford the crude product. The crude product was further purified by flash column chromatography on silica gel with PE and DCM mixture (v/v = 3:1) as the eluent to afford OPOSS-N_3 (6.2 g, 69%) as a clear viscous liquid.

3.9 OPOSS-N_3'

OPOSS-OH' (7.5 g, 5.45 mmol), 4-Azidobenzoic acid (1.33 g, 8.2 mmol) and DMAP (100.1 mg, 0.82 mmol) were added followed by the addition of 50 mL freshly dried THF to dissolved the reactant. Then the mixture was cooled to 0 °C. With stirring, DIPC (1.26 mL, 8.2 mmol) was added dropwise into the mixture. The resulting mixture was stirred for 24 h at room temperature. Then the

THF was fully removed by rotary evaporation afford the crude product. The crude product was further purified by flash column chromatography on silica gel with PE and DCM mixture (v/v = 3:1) as the eluent to afford OPOSS-N_3' (4.4 g, 54%) as a clear viscous liquid.

3.10 Benzene-(Alkyne)$_2$

Hydroquinonemethyl (2.2 g, 20 mmol), propargyl bromide (80% wt in toluene, 4.8 mL, 44 mmol) and K_2CO_3 (11.0 g, 80 mmol) were added in 100mL acetone. After 14 hours of heating reflux, the solid was removed by filtration and the acetone was removed by rotary evaporation. The crude product was further purified by flash column chromatography on silica gel with PE and DCM mixture (v/v = 3:1) as the eluent to afford as Benzene-(Alkyne)$_2$ (1.52 g, 73%) as a pale yellow solid.

3.11 Dimer-R

OPOSS-N_3 (2.0 g, 1.37 mmol), 1,4-Diethynylbenzene (69.2 mg, 0.55 mmol) and CuBr (6 mg, 0.042 mmol) were added to a flask and then transferred to glove box. 10 mL Toluene was added to dissolve the reagents. Then PMDETA (7 mg, 0.040 mmol) was successively introduced. The reaction was performed at room temperature with stirring for 18 h in glove box. After that, the reaction mixture was subjected to column chromatography with DCM:EA (20:1, v/v) to obtain Dimer-R (1.52 g, 90%) as a pale yellow solid.

3.12 Dimer-SR

OPOSS-N_3 (2.0 g, 1.37 mmol), Benzene-(Alkyne)$_2$ (102.1 mg, 0.55 mmol) and CuBr (6 mg, 0.042 mmol) were added to a flask and then transferred to glove box. 10 mL Toluene was added to dissolve the reagents. Then PMDETA (7 mg, 0.040 mmol) was successively introduced. The reaction was performed at room temperature with stirring for 18 h in glove box. After that, the reaction mixture was subjected to column chromatography with DCM:EA (20:1, v/v) to obtain Dimer-SR (1.55 g, 88%) as a viscous solid.

3.13 Dimer-R'

OPOSS-N_3' (2.0 g, 1.33 mmol), 1,4-Diethynylbenzene (69.2 mg, 0.55 mmol) and CuBr (6 mg, 0.042 mmol) were added to a flask and then transferred to glove box. 10 mL Toluene was added to dissolve the reagents. Then PMDETA (7 mg, 0.040 mmol) was successively introduced. The reaction was performed at room temperature with stirring for 18 h in glove box. After that, the reaction mixture was subjected to column chromatography with DCM: EA (20:1, v/v) to obtain Dimer-R' (1.51 g, 90%) as a pale yellow solid.

3.14 Dimer-SR'

OPOSS-N_3' (2.0 g, 1.33 mmol), Benzene-(Alkyne)$_2$ (99.2 mg, 0.53 mmol) and CuBr (6 mg, 0.042 mmol) were added to a flask and then transferred to glove box. 10 mL Toluene was added to dissolve

the reagents. Then PMDETA (7 mg, 0.040 mmol) was successively introduced. The reaction was performed at room temperature with stirring for 18 h in glove box. After that, the reaction mixture was subjected to column chromatography with DCM: EA (20:1, v/v) to obtain Dimer-SR' (1.63 g, 93%) as a viscous solid.

3.15 L-N_3

Pentanol (1.0 g, 11.34 mmol), 4-Azidobenzoic acid (3.7 g, 22.69 mmol) and DMAP (137.9 mg, 1.13 mmol) were added followed by the addition of 50 mL freshly dried THF to dissolved the reactant. Then the mixture was cooled to 0 °C. With stirring, DIPC (3.5 mL, 22.69 mmol) was added dropwise into the mixture. The resulting mixture was stirred for 24 h at room temperature. Then the THF was fully removed by rotary evaporation afford the crude product. The crude product was further purified by flash column chromatography on silica gel with PE and DCM mixture (v/v = 3:1) as the eluent to afford L-N_3 (2.04 g, 77%) as a clear yellow liquid.

3.16 OPOSS-HR

OPOSS-N_3 (2.0 g, 1.37 mmol), Phenylacetylene (167.7 mg, 1.64 mmol) and CuBr (6 mg, 0.042 mmol) were added to a flask and then transferred to glove box. 10 mL Toluene was added to dissolve the reagents. Then PMDETA (7 mg, 0.040 mmol) was successively introduced. The reaction was performed at room temperature with stirring for 18 h in glove box. After that, the reaction mixture was subjected to column chromatography with DCM: EA (20:1, v/v) to obtain OPOSS-HR (1.83 g, 86%) as a clear viscous liquid.

3.17 OPOSS-L-Alkyne

OPOSS-N_3 (2.91 g, 2.0 mmol), 1,4-Diethynylbenzene (504 mg, 4 mmol) and CuBr (6 mg, 0.042 mmol) were added to a flask and then transferred to glove box. 10 mL Toluene was added to dissolve the reagents. Then PMDETA (7 mg, 0.040 mmol) was successively introduced. The reaction was performed at room temperature with stirring for 18 h in glove box. After that, the reaction mixture was subjected to column chromatography with DCM: EA (20:1, v/v) to obtain OPOSS-L-Alkyne (1.95 g, 62%) as a clear viscous liquid.

3.18 OPOSS-R

OPOSS-L-Alkyne (2.0 g, 1.26 mmol), L-N_3 (352.3 mg, 1.51 mmol) and CuBr (6 mg, 0.042 mmol) were added to a flask and then transferred to glove box. 10 mL Toluene was added to dissolve the reagents. Then PMDETA (7 mg, 0.040 mmol) was successively introduced. The reaction was performed at room temperature with stirring for 18 h in glove box. After that, the reaction mixture was subjected to column chromatography with DCM: EA (20:1, v/v) to obtain OPOSS-R (1.67 g, 73%) as a yellow solid powder.

Table S4. Molecule weight and polymer dispersity index (PDI)

Samples	M_w	M_n	PDI
OPOSS	1239	1224	1.01
Dimer-S	4783	4535	1.05
Dimer-SR	3317	3344	1.01
Dimer-R	3413	3380	1.01
Dimer-SR'	3395	3365	1.01
Dimer-R'	3693	3657	1.01

4. NMR data and MS data

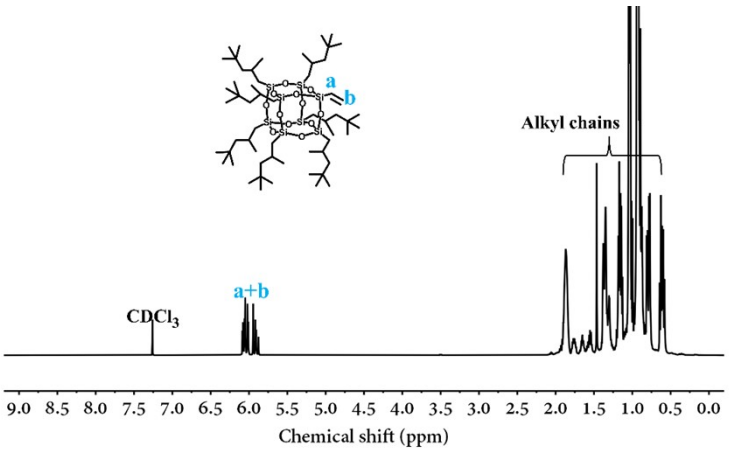

Fig. S19. ^{1}H NMR spectrum of OPOSS-Vinyl.

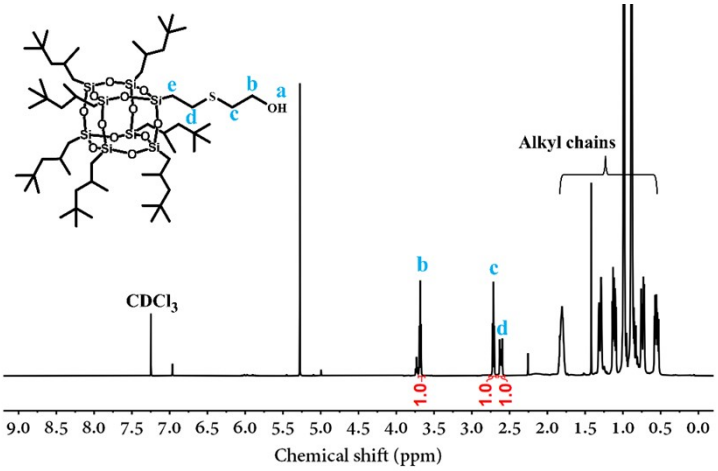

Fig. S20. ^{1}H NMR spectrum of OPOSS-OH.

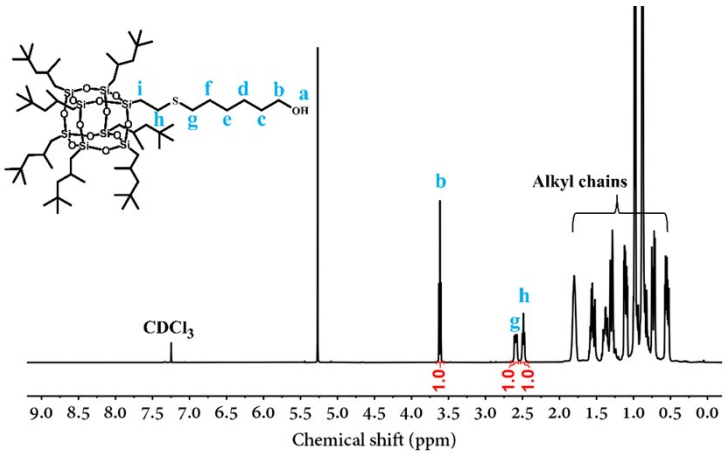

Fig. S21. ^{1}H NMR spectrum of OPOSS-OH'.

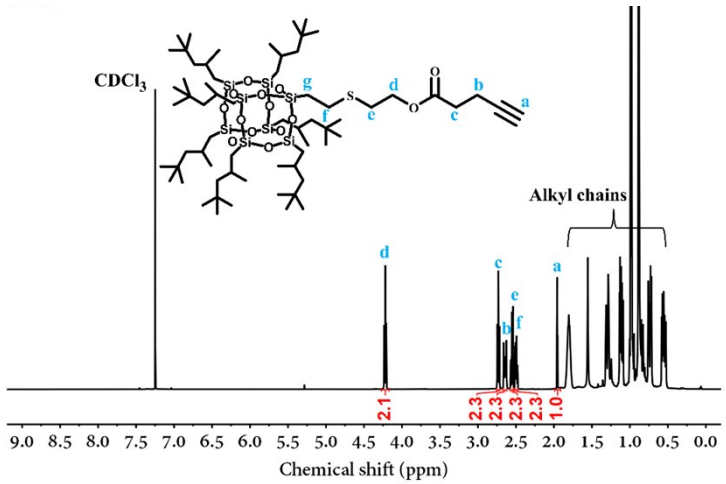

Fig. S22. ^{1}H NMR spectrum of OPOSS-Alkyne.

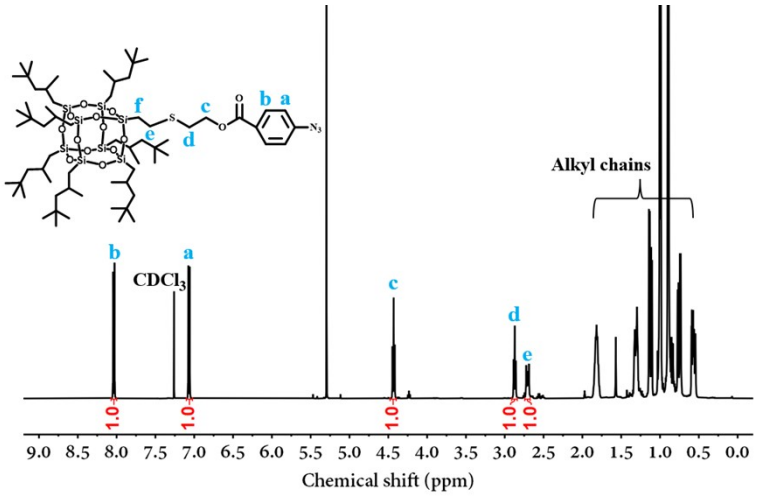

Fig. S23. ^{1}H NMR spectrum of OPOSS-N_3.

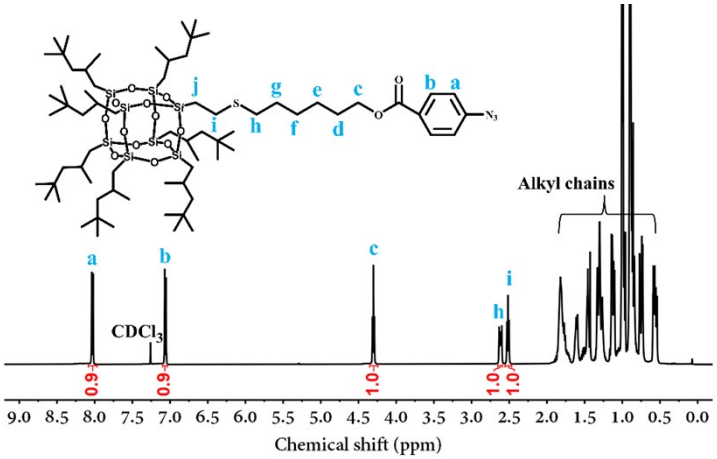

Fig. S24. ^{1}H NMR spectrum of OPOSS-N_3'.

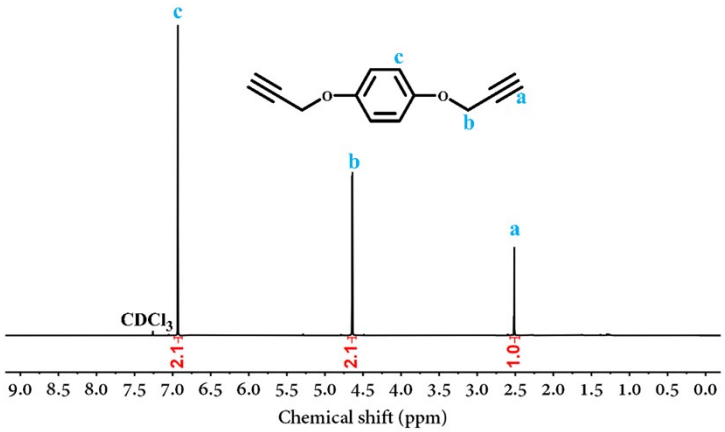

Fig. S25. ^{1}H NMR spectrum of Benzene-(Alkyne)$_2$.

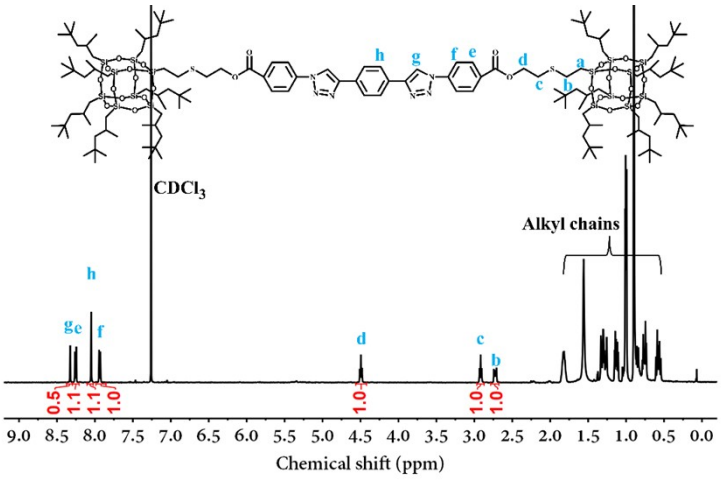

Fig. S26. ^{1}H NMR spectrum of Dimer-R.

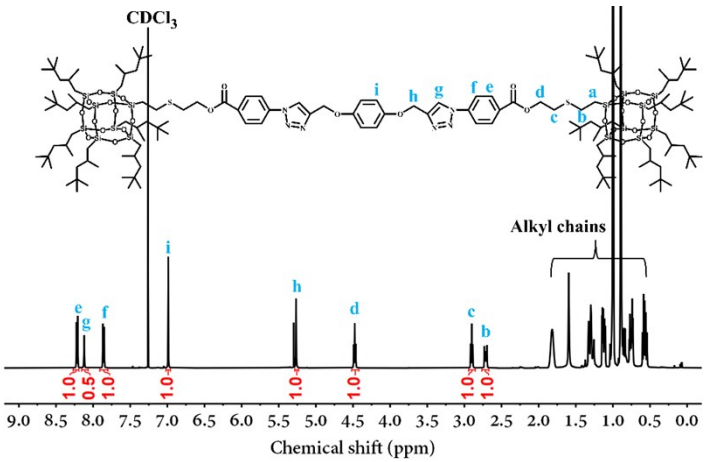

Fig. S27. ^{1}H NMR spectrum of Dimer-SR.

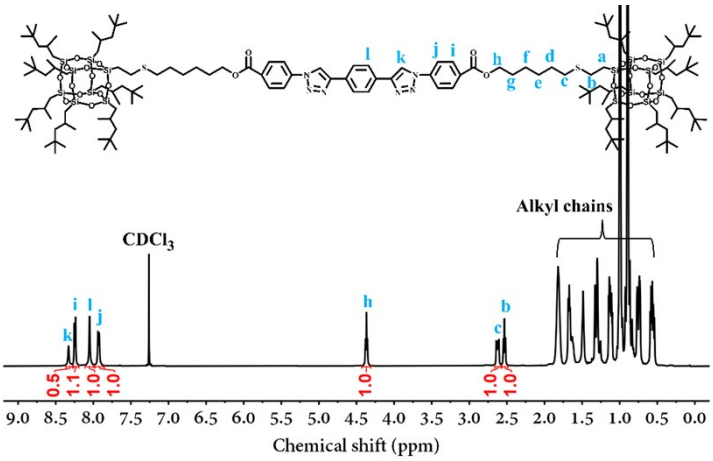

Fig. S28. ^{1}H NMR spectrum of Dimer-R'.

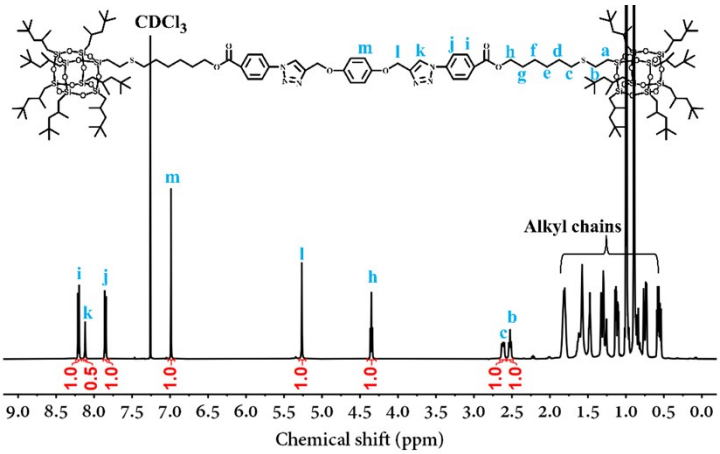

Fig. S29. ^{1}H NMR spectrum of Dimer-SR'.

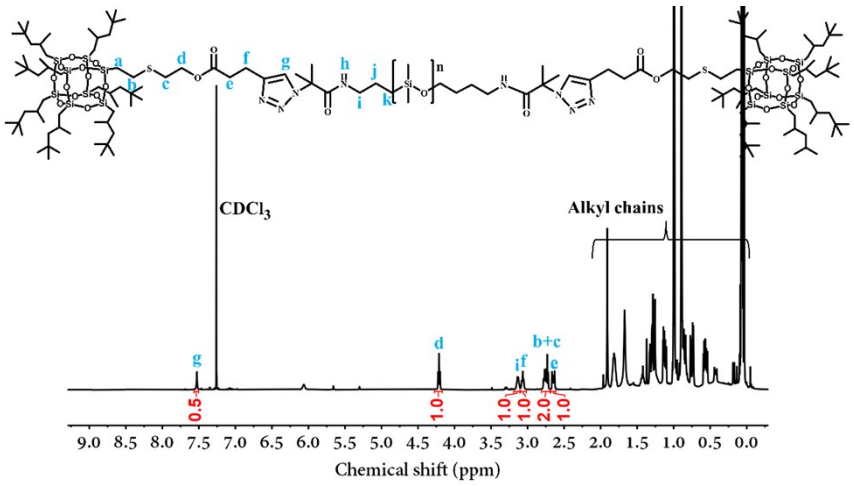

Fig. S30. ^{1}H NMR spectrum of Dimer-S.

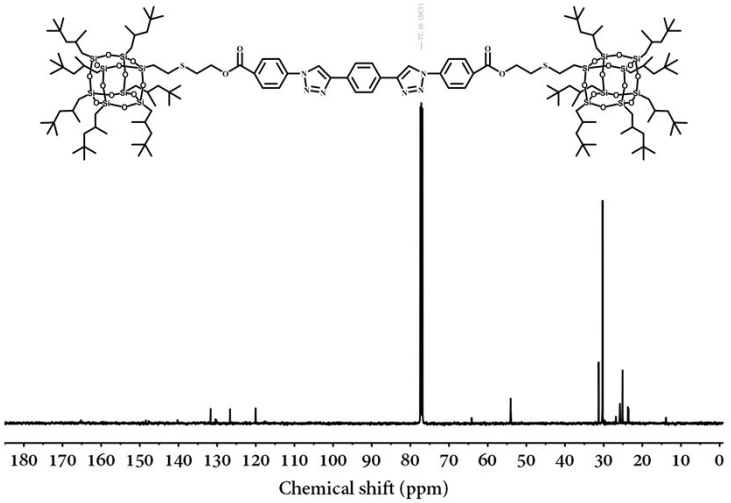

Fig. S31. ^{13}C NMR spectrum of Dimer-R.

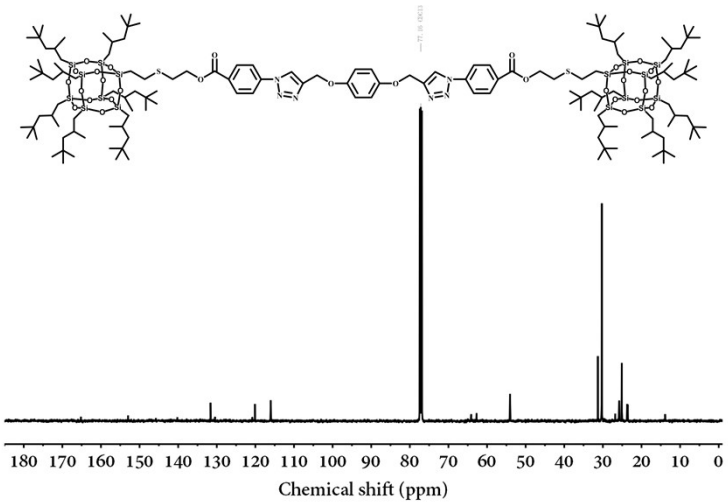

Fig. S32. ^{13}C NMR spectrum of Dimer-SR.

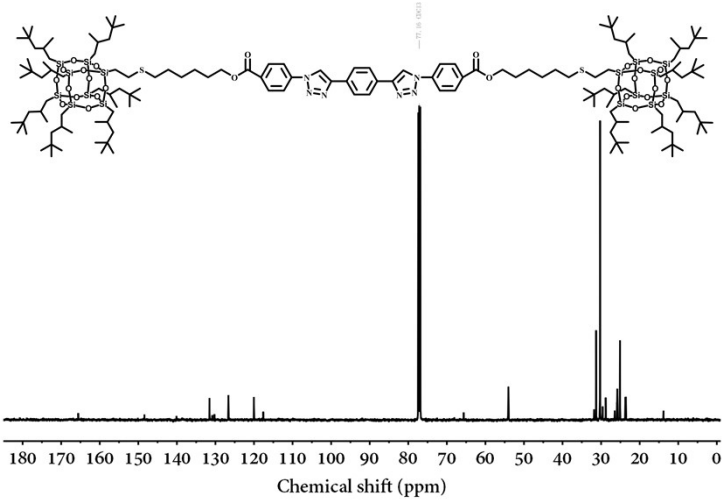

Fig. S33. ^{13}C NMR spectrum of Dimer-R'.

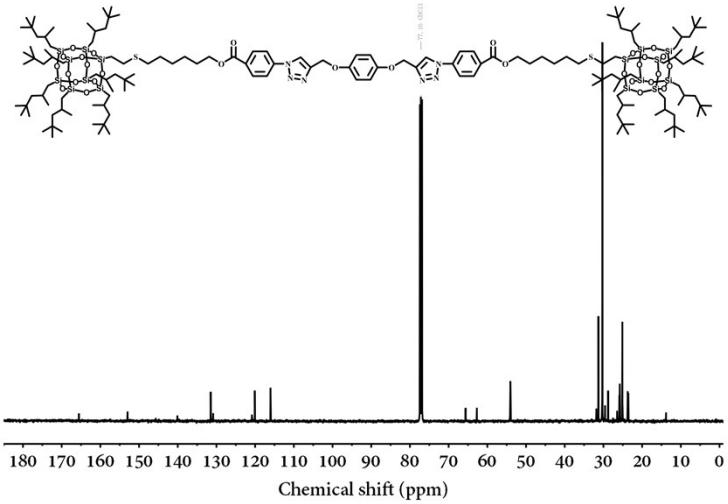

Fig. S34. ^{13}C NMR spectrum of Dimer-SR'.

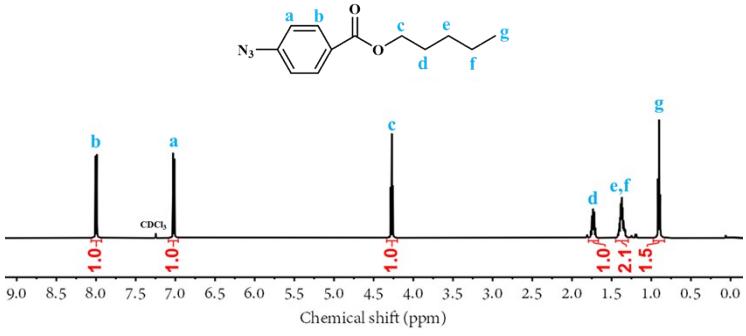

Fig. S35. ^{1}H NMR spectrum of L-N_3.

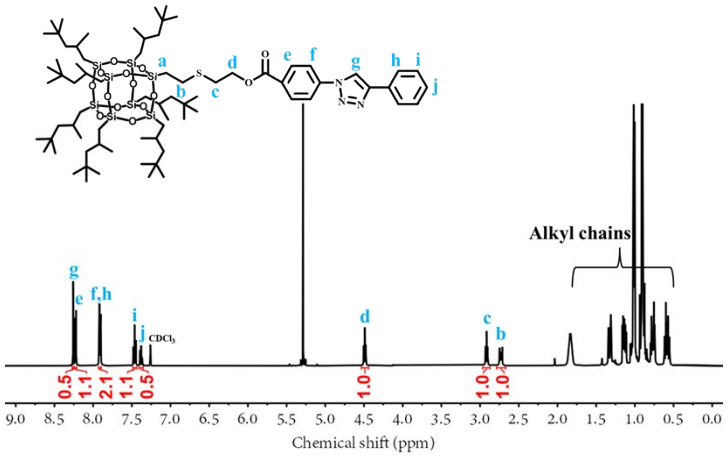

Fig. S36. ^{1}H NMR spectrum of OPOSS-HR.

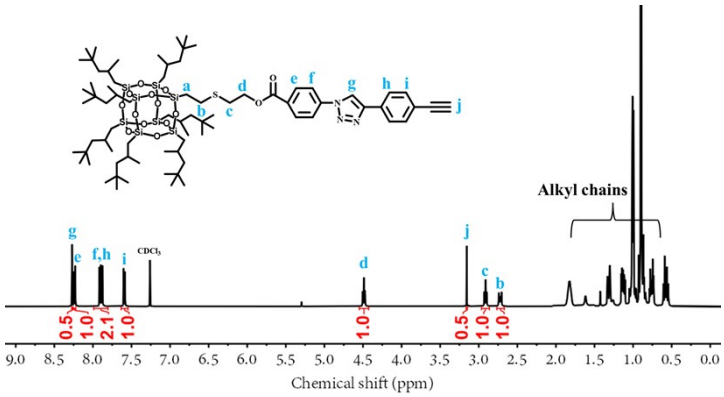

Fig. S37. ^{1}H NMR spectrum of OPOSS-L-Alkyne.

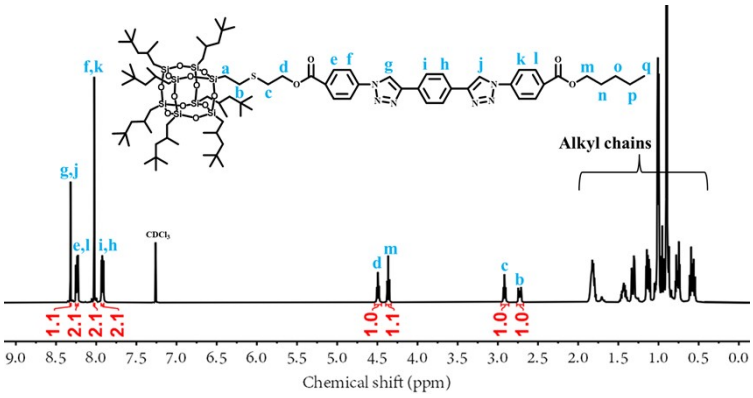

Fig. S38. ^{1}H NMR spectrum of OPOSS-R.

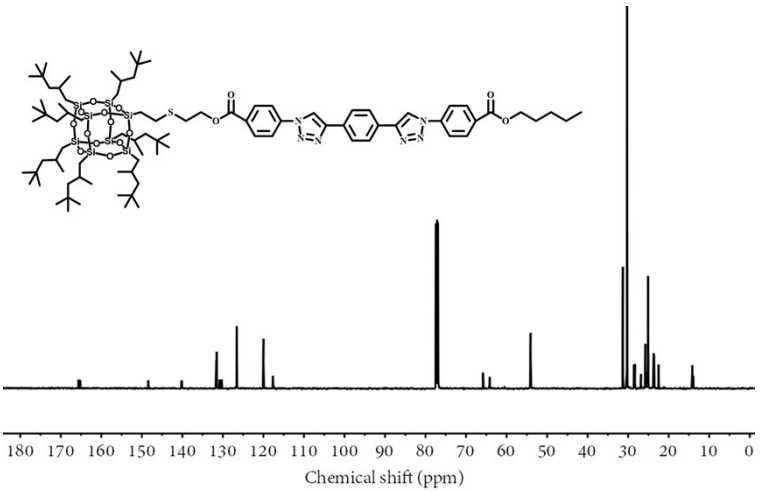

Fig. S39. ^{13}C NMR spectrum of OPOSS-R.

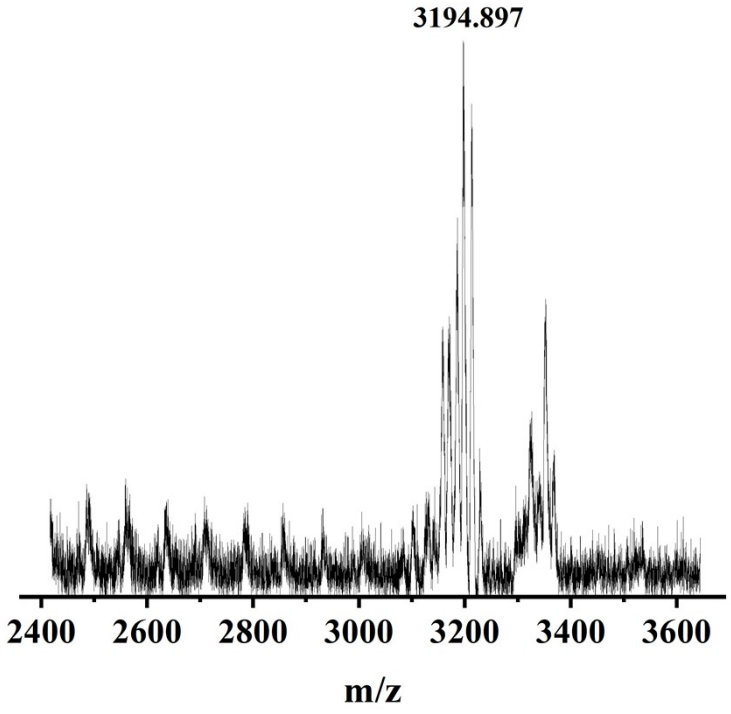

Fig. S40. Mass spectrum of Dimer-R'.

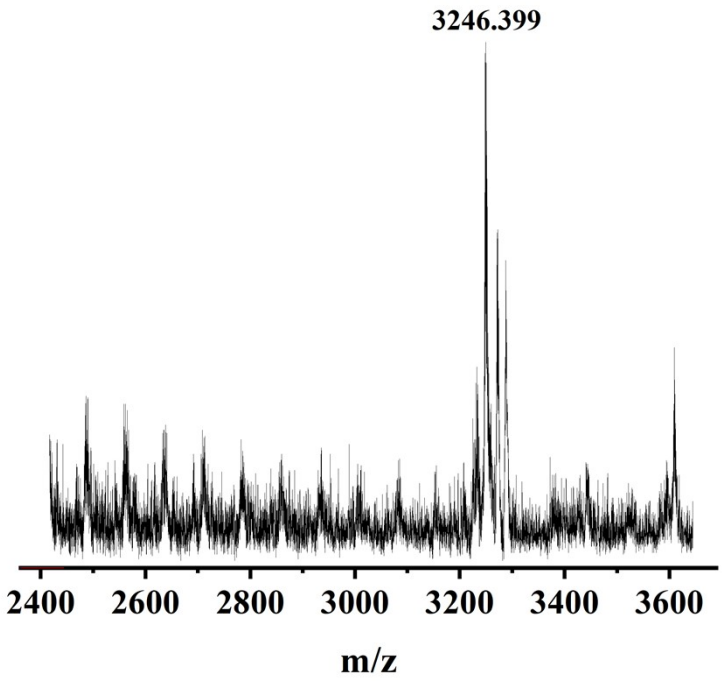

Fig. S41. Mass spectrum of Dimer-SR'.

5. Detail information for SISSO

5.1 Introduction of SISSO

SISSO (Sure Independence Screening and Sparsifying Operators) is an effective method for extracting physical descriptors of huge and potentially correlated features. First developed by Ouyang et al. in 2018, SISSO can automatically find the best descriptor based on a combination of features (i.e. physical properties), making it possible to identify those that are not relevant to a certain issue, so that the feature space can be further optimized. SISSO can not only deal with large spaces while maintaining the efficiency of compressed sensing algorithm (CS), but also can tackle fairly small training test.[1]

5.2. Parameters selection

In our research, we seek to find the mathematical formula between shear viscosity(η) and certain relevant features. During this process, the huge space is first constructed by recursive combinations of input variables and selected mathematical operators. Usually, after three iterations, the number of elements in feature space can reach 10^{10}~10^{12}. The ultra-high-dimensional feature spaces can be reduced by Sure Independence Screening (SIS).[2] SIS scores each feature (standardized) with a metric (correlation magnitude) and keeps only the top ranked. After reducing, SO is applied to identify the best n-dimensional descriptor by sparsifying the linear model of the expanded target property into the feature space.

As illustrated above, we input -cos (θ1), -cos (θ2), Ree (Å), Rg (Å) as our primary features, η (mPa. s) is our target property. The training data for SISSO model building is listed in **Table S2**. After

multiple screenings, we identified the operators used to construct the feature space that minimizes the RMSE: +, -, *, /, sqrt. The size of the SIS-selected subspace is set to be 200000, and the best complexity (the maximal number of operators in a feature) is selected to be 4. Since we only have a small dataset for machine learning (only 4 samples). We confine the descriptor to the lowest dimension of 1D (one coefficient in addition to the intercept in the linear model) to avoid model overfitting.[3]

5.3 Computed result

RMSE (Root Mean Square Error) is a measure of the deviation between the observed value and the true value. It is often used as a standard for measuring the prediction results of machine learning models. One of its advantages is that the dimension of the RMSE is consistent with the target property, but sometimes this feature can also make it difficult to compare different models. The closer the RMSE is to zero, the lower the fit error and the better the regression model.

R^2 is the coefficient of determination of the regression, also known as the goodness of fit, which qualifies the fit of the regression equation to the observed values. It is generally used to compare the performance of models under different dimensions. R^2 is between 0-1, and the larger the value, the better the goodness of fit. Generally, R^2 exceeding 0.9 indicates that the machine learning model is very good.

$$RMSE(X,h) = \sqrt{\frac{1}{m}\sum_{i=1}^{m}\left(h(x_i) - y_i\right)^2} \quad (1)$$

$$R^2 = 1 - \frac{\sum_{i=1}^{n}(p_i - a_i)^2}{\sum_{i=1}^{n}(a_i - \tilde{a})^2} \quad (2)$$

The best descriptor selected by SISSO is :

$$\eta(1D) = 11.67 * \frac{\cos(\theta_2)\sqrt{cos\theta_1}}{cos\theta_1 + cos\theta_2} + 29.50 \quad (3)$$

The RMSE of the model is 0.333584 and R^2 is 0.99938, the fitting plots of both 1D and 2D descriptors are compared in **Fig. S42**. These metrics confirm that our model is a really good one. Although the second dimension leads to a slight improvement in regression performance on the experimental dataset compared to the 1D descriptor, it increases the risk of overfitting and makes it more difficult to promote physical interpretation. So, it is confirmed that the shear viscosity(η) is associated with only rotational stiffness (-cos(θ1) and -cos(θ2)) of dimer linkers, which is consistent with the experimental results.

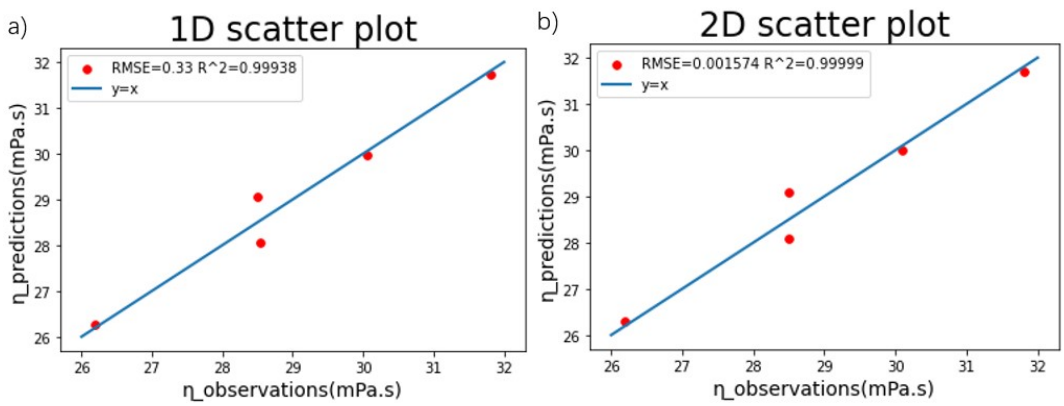

Fig. S42. The fitting plot of the machine learning model. (a) 1D best descriptor (equation 3) for η .(b) 2D best descriptor. The x-axis shows experimental values of η and y-axis shows the predicted values of η according to the best descriptor selected.

5.4 Potential of overfitting

Typically, to evaluate the predictive ability of a model, it is necessary to test it on data that was not used for training. Otherwise, one can incur the so-called overfitting or underfitting. In statistical learning,[4] this is accomplished through cross-validation (CV), a class of techniques that, by dividing the data set into a training and test set in different ways. In CS, dedicated CV techniques are available.[5] Specifically, in a CS-based iterative technique such as SISSO, the model is trained on the training data and the RMSE is evaluated on the test set, the only source of overfitting can come from an overly large size of the descriptor dimensions.[1] Since the dimension of the best descriptor is only one, it is too simple to overfit the data. An estimated 0.33 RMSE achieved by our model shows the good generalization ability of the best descriptor.

5.5 Computer packages used

SISSO was performed using Fortran 90. Data visualizations were generated within the Python package Matplotlib. The SISSO code is open source and can be found at github.com/rouyang2017/SISSO.[1]

5.6 References

1 R. Ouyang, S. Curtarolo, E. Ahmetcik, M. Scheffler and L. M. Ghiringhelli, *Phys. Rev. Mater.*, 2018, **2**, 083802.
2 J. Fan and J. Lv, *J. R. Stat. Soc. B*, 2008, **70**, 849-911.
3 F. Jiang, N. Song, R. Ouyang and P. Ding, *ACS Appl. Mater. Interfaces*, 2021, **13**, 7556-7566.
4 S. G. West and T. Koch, *Struct. Equ. Modeling.*, 2014, **21**, 161-166.
5 R. Ward, *IEEE Trans. Inf. Theory*, 2009, **55**, 5773-5782.